scientific reports

Check for updates

OPEN

Impact of the 2022 heatwave and 2023 extreme summer snowfall on the mass balance of the Chhota Shigri Glacier, western Himalaya

Himanshu Kaushik[1], Mohd. Farooq Azam[1,2]✉ & Md. Arif Hussain[1]

In summer 2022, extreme heatwaves affected many mountain ranges across the Northern Hemisphere—including the Himalaya, Alps, Rockies, and Tibetan Plateau—causing exceptional glacier mass loss. Chhota Shigri Glacier, a benchmark site for long-term monitoring in the western Himalaya, has recorded an average mass balance of − 0.47 ± 0.19 m w.e. a^{-1} over 2002–2023. The 2021–22 hydrological year was characterized by pronounced spring and summer warming, resulting in the most negative annual mass balance in the observational record (–1.71 ± 0.24 m w.e. a^{-1}). In contrast, the following year (2022–23) exhibited a slightly positive mass balance (0.22 ± 0.27 m w.e. a^{-1}), despite 2023 registering the highest global mean temperature on record. This anomalous outcome was associated with cooler spring conditions (–1.16 °C anomaly) and exceptionally high summer precipitation. A major snowfall event in July 2023 delivered > 300 mm of precipitation over three days during the peak ablation season, increasing surface reflectivity and coinciding with a marked reduction in modeled melt. Although not derived from a full surface energy balance analysis, multiple independent indicators consistently support the interpretation of snowfall-induced melt suppression. Contrasting years such as 2021–22 and 2022–23 underscore the growing dominance of extreme weather events under continued warming. While positive mass balance years, such as 2022–23, represent a blip in the long-term glacier wastage trend, they should not be misinterpreted as a sign against ongoing climate change.

Keywords Heatwave, Extreme event, Climate change, Glacier mass balance, Summer snowfall

Glaciers are among the most visible indicators of climate change, with their annual and seasonal mass balance providing a direct response to fluctuations in temperature and precipitation[1–3]. Over recent decades, a persistent trend of negative mass balances has been observed across most of the world's glaciers, primarily driven by ongoing global warming[4–6]. The past decade has been the warmest on record, with global mean temperatures in 2022, 2023, and 2024 exceeding pre-industrial levels by 1.15 °C, 1.45 °C, and 1.55 °C, respectively[7,8]. Correspondingly, global glacier mass loss rates have nearly doubled from − 0.27 ± 0.12 m w.e. a^{-1} during 1976–2014 to − 0.57 ± 0.10 m w.e. a^{-1} in the most recent decade (2015–2024)[4,6].

While long-term glacier mass-balance trends and seasonal climatic controls are well documented, the extent to which short-duration extreme weather events can dominate annual glacier-wide mass balance remains poorly constrained, particularly in the Himalaya, where high-frequency in-situ observations are scarce. In recent years, short-lived extremes have intensified worldwide and have produced glacier mass losses comparable to entire ablation seasons. For example, exceptional heatwaves in 2022 caused unprecedented glacier melt across Europe, Central Asia, and the Himalaya, with Switzerland losing ~ 35% of its seasonal melt within 25 days and glaciers such as Hintereisferner (Austria) and Urumqi No. 1 (China) experiencing record mass loss[9–11].

While temperature extremes are well studied for their role in glacier and snowpack melt, extreme precipitation, though less spatially coherent, is increasingly recognized as a key driver of glacier mass balance[12–16]. However, recent studies, including the "Sixth Assessment Report of IPCC" confirm that the frequency and intensity of extreme precipitation events are increasing across many regions due to anthropogenic climate change. In recent decades, the Himalaya and Tibetan Plateau have experienced numerous such extreme precipitation events[17–19].

[1]Department of Civil Engineering, Indian Institute of Technology Indore, Indore 453552, India. [2]International Centre for Integrated Mountain Development, Kathmandu, Nepal. ✉email: farooqaman@yahoo.co.in; farooqazam@iiti.ac.in

Precipitation in the Himalayan region is primarily governed by western disturbances (WDs) during winter and the Indian Summer Monsoon (ISM) during summer[20]. In the western Himalaya, winter precipitation is traditionally dominated by WDs originating from the Mediterranean region[21–23]. However, recent studies report a decline in winter WD frequency accompanied by increased WD activity during the pre-monsoon and early monsoon months (May–July)[21–24]. This evolving seasonal overlap between WDs and the ISM enhances the likelihood of short-lived but intense precipitation events, sometimes leading to cascading hydrological hazards[15,24,25]. Such anomalous summer precipitation can also strongly affect glacier surface processes, particularly when snowfall temporarily increases surface albedo and suppresses melt[16].

When contrasting short-lived extremes occur in succession, their combined influence can strongly modulate interannual glacier mass balance. An extreme melt season driven by a heatwave can precondition the glacier surface by depleting seasonal snow and lowering albedo, thereby enhancing sensitivity to subsequent weather anomalies[16,26,27]. Conversely, an exceptional summer snowfall following a high-melt year can abruptly suppress ablation and partially offset earlier mass loss. Despite this potential for sequence-dependent glacier responses, most existing studies examine temperature extremes or precipitation anomalies independently, leading to uncertainty in attributing annual glacier-wide mass-balance anomalies to specific short-duration events or their sequencing[9,10,26–28]. As a result, the capacity of consecutive short-duration extremes to temporarily override longer-term climatic forcing remains insufficiently understood, particularly in the western Himalaya.

Chhota Shigri Glacier, a benchmark glacier in the western Himalaya, has been extensively monitored and provides one of the longest in-situ mass-balance records in the region[16,29–31]. While previous studies have established its long-term mass-balance evolution and sensitivity to seasonal temperature and precipitation variability, the role of short-duration extreme events and their combined, event-scale influence on annual glacier-wide mass balance remains inadequately constrained.

Building on this foundation, the present study explicitly links hourly-to-daily-scale temperature and precipitation extremes with glacier mass-balance responses during two consecutive and contrasting hydrological years. Specifically, we examine how an early spring–summer heatwave in 2022, followed by exceptionally high summer snowfall in 2023, interacted to control glacier-wide annual mass balance. The objectives are to: (1) assess how such event sequences influence annual glacier-wide mass balance, and (2) quantify the glacier's event-scale mass-balance response using a temperature-index model driven by high-resolution in-situ glacio-meteorological observations.

Study site

The Chhota Shigri Glacier (32.28°N, 77.58°E) is a valley-type glacier located in the western Himalaya, Himachal Pradesh, India (Fig. 1). It covers an area of 15.5 km² of glacierised area and descends from 5830 m to 4072 m above sea level. The glacier feeds the Chandra River, a tributary of the Chenab (Indus) River. It is a non-surging, temperate glacier, primarily composed of clean ice with approximately 12% debris cover[29]. The glacier receives 33% of its annual precipitation from the ISM during summer (June–September), and 67% from WDs in winter (October–May), with a mean annual precipitation of 922 mm[32]. The winter period was further subdivided into spring (March–May) and autumn (October–November) seasons for the meteorological analysis. Continuous monitoring since 2002 has established Chhota Shigri as a benchmark glacier. Satellite and field observations (Fig. 2) reveal substantial surface changes following the 2022 heatwave, highlighting the glacier's high sensitivity to extreme weather events. Moreover, a recent study[33] also suggested that this glacier is a representative glacier for the whole western Himalaya.

Results and discussion

Contrasting glacier mass balance responses during 2021–22 and 2022–23

High-frequency in-situ observations from Chhota Shigri Glacier reveal pronounced interannual variability in glacier-wide mass balance driven by short-duration temperature and precipitation extremes. The results are interpreted at the event scale, emphasizing short-duration climate anomalies rather than regional mean behaviour or long-term trends. Long-term monitoring indicates a mean annual mass loss of – 0.47 ± 0.19 m w.e. a^{-1}[29]. In contrast, the hydrological year 2021–22 recorded the most negative mass balance on record (– 1.71 ± 0.24 m w.e. a^{-1}), while 2022–23 exhibited a slightly positive mass balance (0.22 ± 0.27 m w.e. a^{-1}), highlighting exceptional year-to-year variability (Fig. 3a).

The 2021–22 glacier-wide mass balance lies above the 95th percentile of the 2003–2023 observational period, whereas the slightly positive balance in 2022–23 falls below the 90th percentile, despite 2023 being the warmest year globally[8]. Among globally monitored glaciers, only one glacier in Antarctica recorded a slightly positive mass balance in 2023 (Fig. 3b); direct comparison is not meaningful due to Antarctica's opposite seasonal cycle and distinct climatic regime. Notably, Chhota Shigri was the only monitored glacier in the western Himalaya to show a positive annual balance in 2022–23. Other regional glaciers exhibited a clear reduced mass losses relative to 2021–22 but did not attain a positive mass balance[34,35].

For example, Gepang Gath Glacier, located in the same basin as Chhota Shigri, recorded – 0.55 ± 0.37 m w.e. a^{-1} in 2022–23 compared to – 1.30 ± 0.39 m w.e. a^{-1} in 2021–22, approximately 50% less negative, indicating a significant reduction in melt within the same basin[34]. Similarly, Drang Drung Glacier in the western Himalaya showed a decrease from – 1.09 ± 0.43 to – 0.38 ± 0.43 m w.e. a^{-1} (~ 65% less negative) over the same period[35], indicating a broader regional signal of reduced ablation linked to anomalous weather conditions. In contrast, several glaciers in the central and eastern Himalaya (e.g., Mera, Pokalde, and Yala) continued to experience extreme mass losses, underscoring the heterogeneous influence of summer precipitation anomalies across the Himalayan arc[36].

To further understand the processes underlying this exceptional interannual contrast at Chhota Shigri Glacier, we examine melt behaviour across different surface types, including debris-covered ice, using point-

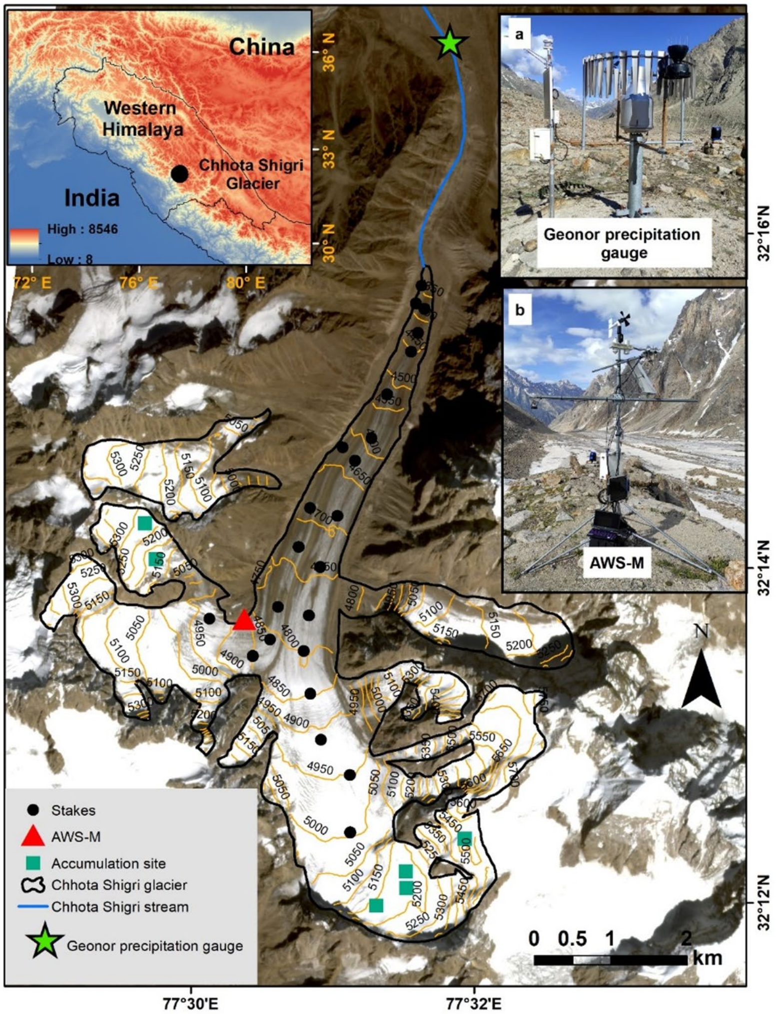

Fig. 1. Chhota Shigri Glacier showing ablation and accumulation measurement sites. Background: PlanetScope image, 20 Oct 2023. Panels **(a)** Geonor precipitation gauge; **(b)** AWS-M.

scale mass-balance observations. Approximately 12–15% of Chhota Shigri Glacier is debris-covered[29], which can modulate melt rates depending on debris thickness and prevailing meteorological conditions. Although debris energy-balance processes are not explicitly resolved here, point mass-balance measurements from debris-covered elevations reveal pronounced contrasts between the two years. During the 2022 heatwave, melt at debris-covered sites (4263–4360 m a.s.l.) ranged from − 4.23 to − 7.01 m w.e., whereas during the anomalous summer snowfall year of 2023, melt was reduced to − 2.11 to − 3.80 m w.e., corresponding to a 45–50% decrease. Importantly, a similar reduction in melt was observed over clean-ice areas, indicating that enhanced summer snowfall and associated snow cover, rather than debris-specific insulation effects, were the dominant control on seasonal melt reduction. These observations highlight the primary role of short-duration atmospheric forcing—particularly snowfall versus sustained heat—in governing interannual melt variability across both debris-covered and clean-ice surfaces. The absence of debris thickness measurements and explicit energy-balance partitioning limits further attribution, underscoring the need for future studies combining debris mapping with surface energy-balance observations.

The altitudinal distribution of point mass balance exhibits a clear elevation dependence in both years (Fig. 3c). Linear regressions yield vertical mass-balance gradients (db/dz) of 0.76 m w.e. (100 m)$^{-1}$ in 2021–22 and 0.61 m w.e. (100 m)$^{-1}$ in 2022–23. The higher equilibrium-line altitude in 2021–22 (5213 m a.s.l.) reflects enhanced melt during the heatwave year, whereas the lower ELA in 2022–23 (4992 m a.s.l.) indicates moderated ablation under cooler conditions and increased summer snowfall. Comparable reductions in db/dz during 2023 have been reported for other western Himalayan glaciers[34,35], suggesting a coherent regional response to interannual variability in melt-season climate.

Interpretation of these results is subject to limitations inherent to single-site studies. Climatic heterogeneity across the Himalaya, glacier-type variability, and local forcing factors—including debris distribution, glacier hypsometry, slope-aspect controls on radiation receipt, and interactions between WDs and the ISM—can strongly modulate glacier responses to short-duration extremes. Consequently, the magnitudes reported here

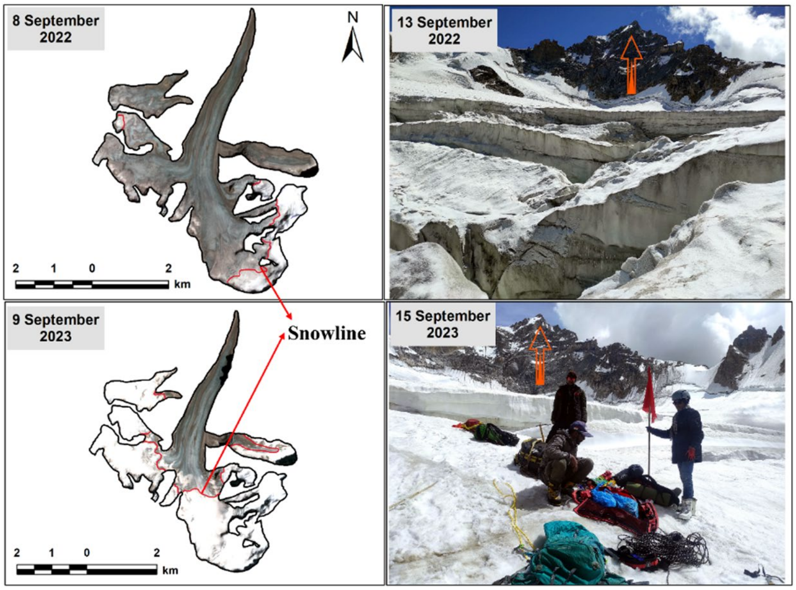

Fig. 2. Chhota Shigri Glacier surface changes after the 2022 heatwave and one year later. Left: PlanetScope satellite images (3 m resolution) on 8 Sep 2022 and 9 Sep 2023. Right: Ground photographs from the exact location on 13 Sep 2022 and 15 Sep 2023, highlighting the changes in the glacier's surface condition.

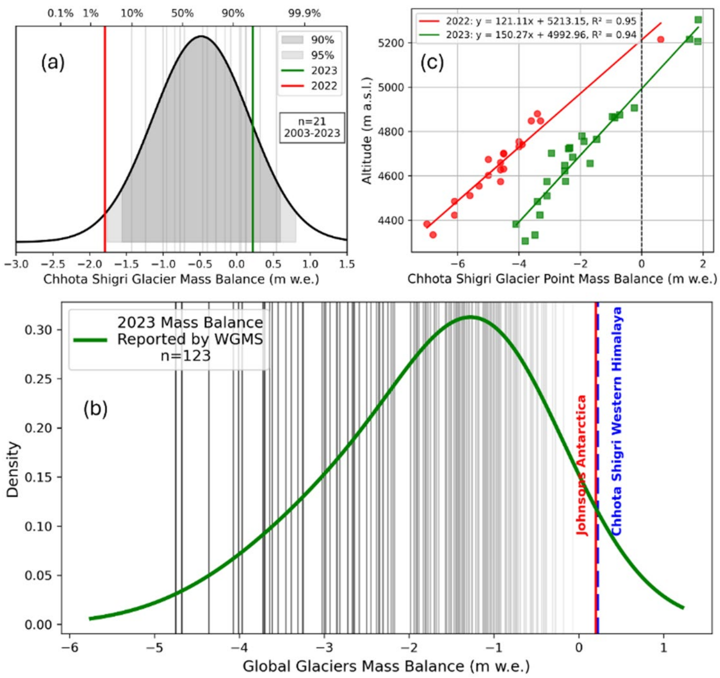

Fig. 3. Mass balance of Chhota Shigri Glacier. **(a)** The vertical grey line shows the annual mass balance from 2003 to 2023, overlaid on a generalized extreme value distribution. Shaded areas represent the 90% and 95% quantiles. **(b)** Global glacier mass balance in 2023: WGMS data for 123 glaciers with kernel density estimation fit. Vertical grey lines (light to dark) show glacier-wise mass balance from least to most negative. **(c)** Altitudinal distribution of point mass balance for the hydrological years 2021–22 (red) and 2022–23 (green), with corresponding linear fits used in this study.

should not be interpreted as regionally representative, but rather as process-based evidence illustrating how short-lived meteorological extremes can temporarily dominate annual glacier-wide mass balance under specific local conditions.

Extreme warming during spring and summer 2022 at AWS-M

Exceptional air temperatures were recorded at the AWS-M site (4,863 m a.s.l.) during spring (March–May) and summer (June–September) 2022, with two prolonged warm spells clearly evident in the hourly temperature record (Fig. 4a). These occurred during 13 March–13 April (spring) and 26 June–13 July (summer) and were characterized by sustained positive anomalies relative to the 2010–2021 reference period. Daily temperature anomalies during the spring warm spell frequently reached 4–6 °C, while summer anomalies were typically 2–3 °C (Figs. 4b–c). Diurnal temperature cycles further highlight the event intensity, with mean diurnal temperatures during both warm spells 5–6 °C higher in 2022 than in 2023 (Figs. 4d–e).

A percentile-based analysis at both hourly and daily scales (90th, 95th, 97.5th, and 99th percentiles; Fig. 5; Supplementary Fig. S2; Table S1) confirms the exceptional duration and intensity of the 2022 heatwave. During both warm spells, temperatures consistently exceeded the 90th and 95th percentiles and frequently crossed the 97.5th and 99th percentiles. The spring warm spell (13 March–13 April 2022) was particularly extreme, with a mean air temperature of − 4.75 °C, 5.12 °C warmer than the same period in 2023 (− 9.87 °C), representing the highest value in the 2010–2023 record (Supplementary Table S2). During the summer warm spell (26 June–13 July), mean air temperature reached 6.00 °C, more than twice that observed in 2023 (2.77 °C) for the same period.

Although the percentile thresholds were derived from a relatively short reference climatology (2010–2021) that overlaps with a period of regional warming—thereby elevating the threshold values—the 2022 warm spells

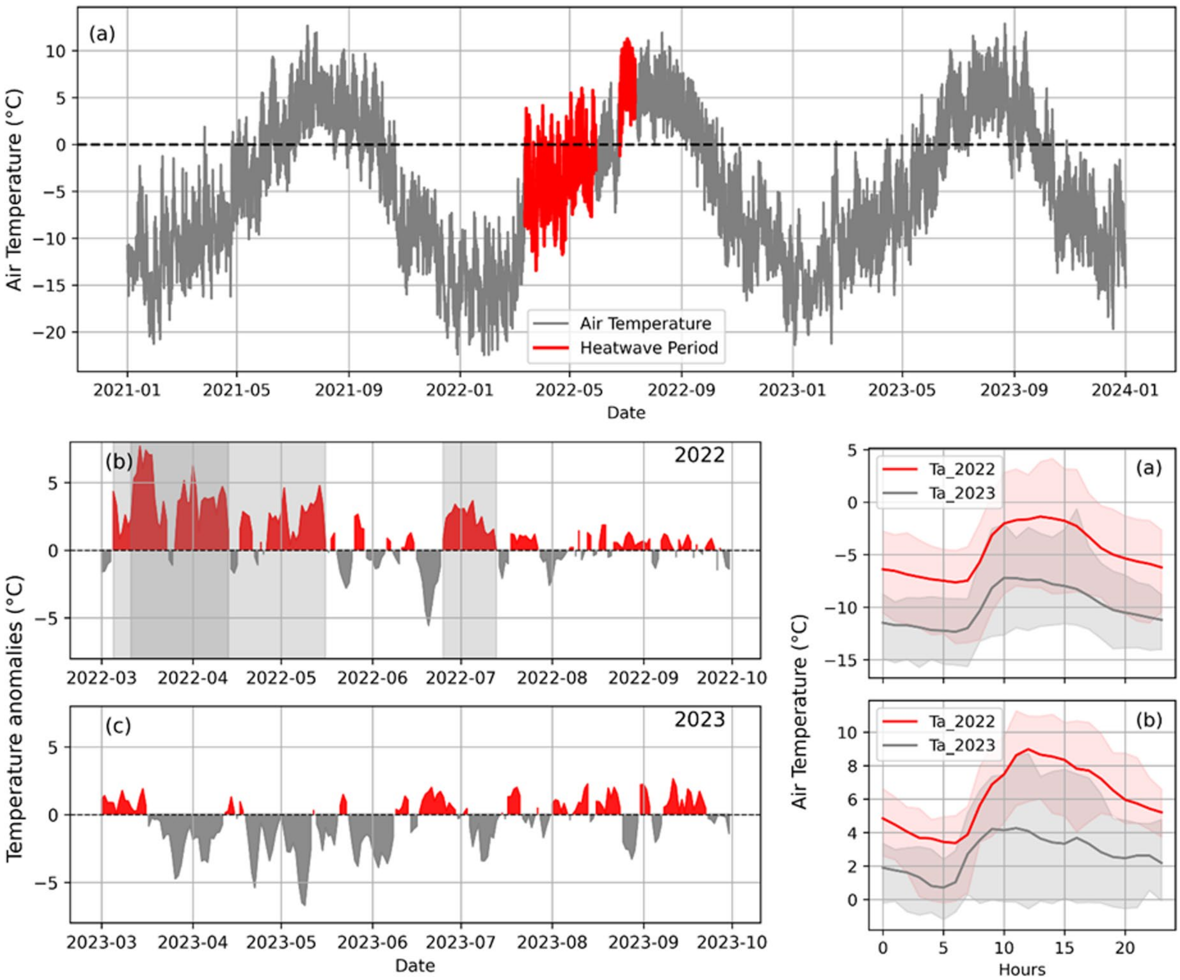

Fig. 4. Air temperature patterns and anomalies at Chhota Shigri Glacier during the 2022 heatwave and 2023. **(a)** Hourly air temperature recorded at 4,863 m a.s.l. from AWS-M between 1 January 2021 and 31 December 2023. The 2022 heatwave periods are highlighted in red. (**b)** Daily temperature anomalies from 1 March to 30 September 2022, with both warm spells in spring and summer, are indicated by grey shading. **(c)** Same as (b), but for 2023. **(d–e)** Diurnal temperature cycles during the two warm spells in 2022, compared with corresponding periods in 2023. Grey shades represent variability.

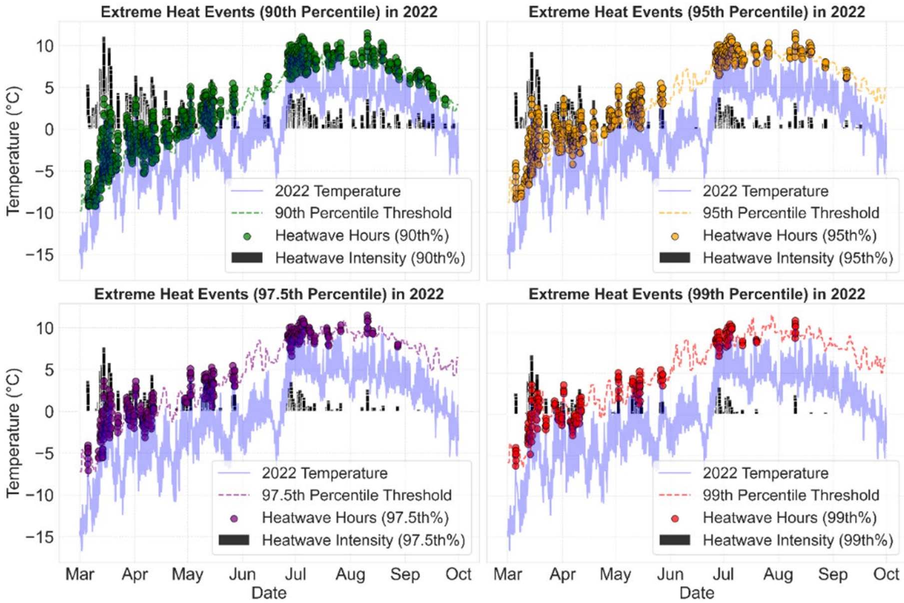

Fig. 5. Hourly temperature percentile thresholds (90th, 95th, 97.5th, 99th), and identification of extreme heatwave hours (≥ 3 consecutive hours above threshold) for 2022.

nevertheless exceeded even the highest percentile levels at both daily and multi-day timescales. This indicates that the events were extreme relative to an already warm baseline. As the analysis emphasizes event persistence and relative exceedance rather than absolute climatological thresholds, identification of 2022 as an exceptional heatwave year remains robust.

The spring warm spell was unprecedented in the observational record, with 103 hours above freezing, a cumulative positive temperature of 121 °C hours, and a mean air temperature of 1.17 °C (Supplementary Fig. S3). ERA5-Land anomalies relative to the 1950–2023 climatology independently confirm the magnitude of this spring warming (Supplementary Fig. S4; Table S3). Occurring during the typical accumulation season, this early warming likely triggered premature snowmelt, reduced snowpack persistence, and lowered surface albedo, thereby preconditioning the glacier for enhanced summer ablation[37–39].

Comparable extreme warming was reported across other glacierized regions during 2022, including glaciers in High Mountain Asia and the European Alps (e.g., Kuoqionggangri, Sangqu, Urumqi No. 1, Findelgletscher, Rhonegletscher, Hintereisferner)[9–11,26], supporting the regional character of this anomaly. These conditions explain why 2021–22 recorded the most negative mass balance at Chhota Shigri Glacier. In contrast, 2022–23, despite being the warmest year globally on record[8], exhibited no above-freezing hours during the same spring window (13 March–13 April; Supplementary Fig. S3), underscoring how regional-scale weather variability can dominate glacier mass-balance outcomes independently of global mean temperature trends[39,40].

Precipitation extremes and their impact on glacier mass balance: the anomalous case of 2023

Glacier mass balance in the Himalaya is controlled not only by air temperature but also by the timing, phase (rain versus snow), and intensity of precipitation events[16,27,28]. During the 2022–23 hydrological year, total precipitation over Chhota Shigri Glacier reached 977 mm, of which 478 mm (49%) occurred during summer. A single, exceptional precipitation event between 8 and 10 July 2023 accounted for > 300 mm, representing ~ 31% of the annual total (Fig. 6a). This event exceeded both the India Meteorological Department (IMD) criteria for heavy to very heavy rainfall and the World Meteorological Organization (WMO) extreme precipitation thresholds, and was likely associated with interactions between Western Disturbances and the Indian Summer Monsoon[19].

Solid precipitation measurements from the Geonor T-200B gauge, equipped with a single Alter wind shield, are subject to wind-induced undercatch during snowfall[40–43]. Results from the WMO Solid Precipitation Intercomparison Experiment (SPICE) indicate that for shielded Geonor gauges operating under snowfall conditions and mean wind speeds of ~ 2–3 m s^{-1}, catch efficiencies typically range between ~ 75–85%[41]. During the 8–10 July event, mean wind speeds at the Geonor site were ~ 2.5–2.8 m s^{-1}, implying a likely underestimation of solid precipitation by ~ 15–25%. Accordingly, the reported snowfall total of ~ 300 mm should be interpreted as a conservative estimate, with a plausible corrected range of ~ 350–400 mm. This uncertainty primarily affects the absolute magnitude of precipitation, while the timing, duration, and phase of the event remain robust. Thus, the occurrence of a short-duration, exceptionally intense summer snowfall is well constrained and sufficient to explain the observed suppression of melt during the peak ablation period.

At higher elevations, most of this precipitation likely fell as snow, as indicated by in-situ data. During 8–10 July, mean air temperatures were – 3.31 °C at high camp and at or below 0 °C at base camp, confirming snowfall

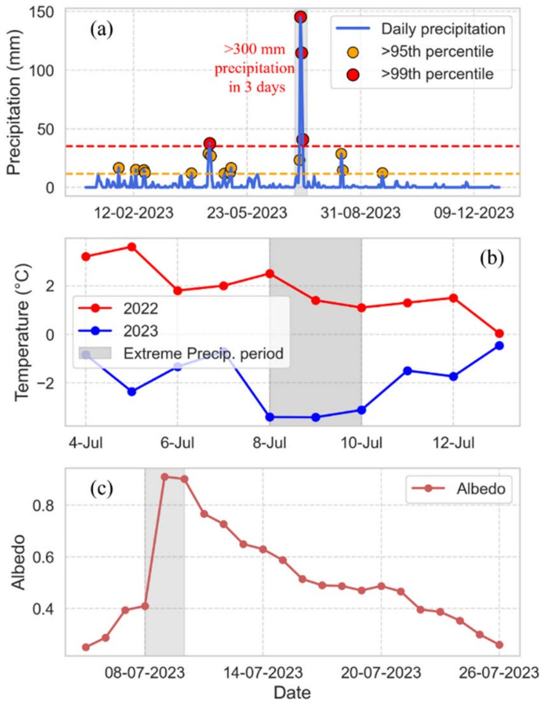

Fig. 6. **(a)** Extreme July 2023 precipitation event showing more than 300 mm accumulated in three days (highlighted by grey shading), with daily totals exceeding the 95th and 99th percentile thresholds. **(b)** Daily mean air temperature during the extreme precipitation period in 2022 and 2023; the grey shaded **(c)** Subsequent increase in glacier surface albedo (6–24 July) following the snowstorm.

rather than rainfall (Fig. 6b). This event triggered a rapid and sustained increase in surface albedo, rising from 0.28 on 6 July (exposed debris) to 0.90 by 9 July, indicative of widespread fresh snow cover (Fig. 6c). Elevated albedo persisted until 24 July, substantially reducing shortwave radiation absorption (Supplementary Fig. S1), delaying ice exposure, and resulting in anomalous mass gain between 6 and 24 July.

Although the AWS-M is located on a lateral moraine and its absolute albedo values may not fully represent glacier-wide conditions, the abrupt magnitude and persistence of the albedo increase provide a robust qualitative indicator of snow-related surface changes. Because snow typically persists longer on glacier ice than on debris-covered moraine due to lower thermal conductivity, the AWS-M record likely represents a conservative proxy for snow-cover persistence and associated radiative effects on the glacier surface.

This event-scale summer snowfall demonstrates that fresh snow can temporarily suppress glacier melt even during peak ablation, emphasizing that summer air temperature is as critical as precipitation amount in governing glacier mass balance. Air temperature controls the precipitation phase at the glacier surface, thereby exerting first-order control on surface albedo and shortwave radiation absorption—the dominant energy source for melt on Himalayan glaciers[16]. Similar melt-suppressing effects of summer snowfall have been documented across multiple mountain regions, including the Alps[44], Andes[45], Tibetan Plateau[27,28,46], Tian Shan[47], Eastern Himalaya[48], Western Himalaya[16], and Karakoram[49].

Earlier work at Chhota Shigri Glacier inferred these processes using lower-elevation (1,559 m a.s.l.) meteorological data from the Bhuntar station (from the Beas basin, ~ 50 km distance)[16]. The present study substantially advances this understanding by employing local, high-altitude observations near the glacier surface, enabling direct resolution of snowfall-induced changes in albedo, shortwave radiation, and mass balance. Together, these observations confirm that extreme summer snowfall can transiently shift the glacier energy balance, highlighting the critical role of precipitation phase—regulated by summer air temperature—in modulating Himalayan glacier mass balance.

Although a full surface energy-balance (SEB) analysis is not performed, the inference that the July 2023 snowfall suppressed melt is supported by multiple independent indicators: **(i)** near-freezing air temperatures during the event, **(ii)** a sharp and sustained increase in surface albedo, and **(iii)** anomalous mass gain and reduced ablation immediately following the snowfall. Collectively, these observations provide robust physical evidence that reduced shortwave radiation absorption substantially limited melt during the peak ablation season, even in the absence of explicit SEB partitioning.

Temperature and precipitation anomalies from in-situ and ERA5 Land data

Monthly temperature and precipitation anomalies were calculated using in-situ observations from the AWS-M station relative to the 2010–2021 reference period (Fig. 7). During the 2021–22 hydrological year, AWS-M recorded a positive annual temperature anomaly of 0.33 °C, with a pronounced 1.01 °C anomaly during the March–September period. Spring (March–May) exhibited the strongest warming, with a 2.02 °C anomaly,

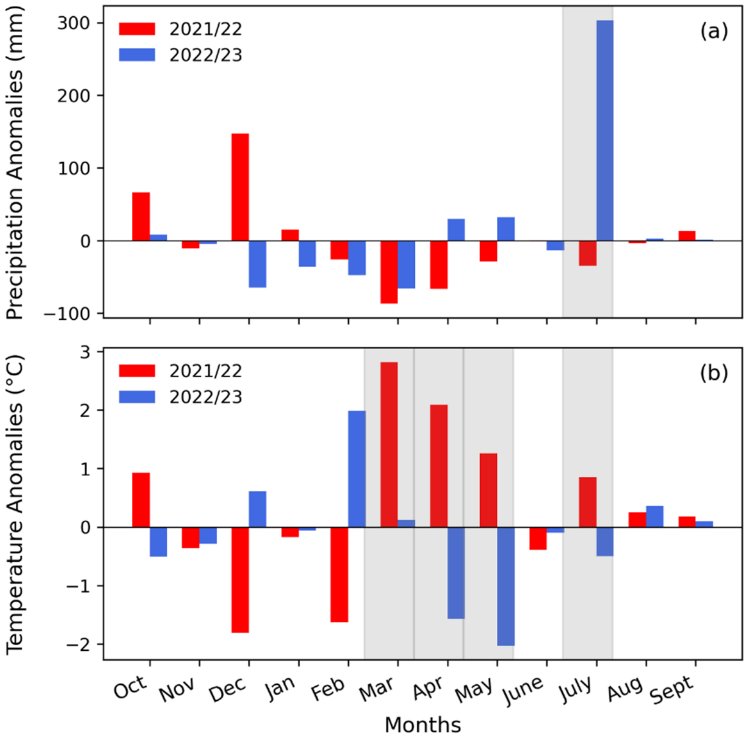

Fig. 7. Mean monthly temperature and precipitation anomalies for 2021–22 and 2022–23 hydrological year's corresponding to the in-situ data (temperature 2010–2021 and precipitation 2012–2021).

the highest spring anomaly in the 14-year AWS-M record (Fig. 7b). In contrast, precipitation anomalies in 2021–22 were negative, with deficits of − 61 mm in spring and − 29 mm in winter (Fig. 7a). The combination of anomalously warm conditions and reduced precipitation explains the strongly negative glacier-wide mass balance observed in 2021–22.

In contrast, the 2022–23 hydrological year was characterized by cooler-than-average conditions, with annual and March–September temperature anomalies of − 0.16 °C and − 0.52 °C, respectively (Fig. 7b). Precipitation anomalies were strongly positive, particularly during summer, which recorded an excess of 260 mm. July alone exhibited an extreme monthly anomaly exceeding 300 mm (Fig. 7a), associated with the exceptional summer snowfall event. Although spring precipitation showed a negligible negative anomaly relative to the long-term mean (− 1 mm), it was 178% higher than in 2021–22, while summer precipitation was 135% higher than in 2021–22, reflecting a pronounced interannual shift in moisture availability.

ERA5-Land reanalysis data (1950–2023) provide broader climatic context for these anomalies (Supplementary Fig. S5). The year 2022 recorded an annual temperature anomaly of 1.70 °C, ranking among the warmest years in the 74-year record and driven by persistent spring and early-summer warming (Supplementary Figs. S4 and S5a). In contrast, 2023, despite being the globally warmest year on record (1.45 °C)[8], showed only a modest regional anomaly of 0.25 °C over the Chhota Shigri Glacier region, highlighting strong spatial heterogeneity in warming signals. ERA5-Land precipitation anomalies corroborate the in-situ observations, identifying 2022 as anomalously dry and 2023 as wetter than average, largely due to the July snowfall event (Supplementary Fig. S5b). While both datasets are consistent in sign and magnitude at seasonal scales, the in-situ Geonor gauge more effectively captures short-lived, high-intensity precipitation extremes.

These temperature and precipitation anomalies provide a coherent climatic explanation for the contrasting glacier mass-balance responses observed during the two hydrological years. A similar pattern—strongly negative mass balances in 2021–22 followed by less negative or moderated losses in 2022–23—was reported for neighboring glaciers within ~ 30 km, including Samudra Tapu, Gepang Gath, and Sutri Dhaka[34,36]. Together, these observations indicate that basin-wide anomalies in temperature and precipitation, rather than purely local effects, played a dominant role in controlling glacier mass balance across the Chandra Basin during this period.

T-index modeling of glacier mass balance under seasonal weather extremes

We applied a temperature-index (T-index) model to simulate glacier-wide mass balance for the hydrological years 2021–22 and 2022–23, resolving both seasonal and annual variability. To ensure physically consistent initial conditions, the model was spun up for a 10-year period (2011–2021) using ERA5-Land temperature and precipitation forcing. This spin-up period allowed the seasonal snowpack and firn layers to equilibrate prior to the analysis years and minimized the sensitivity of the simulations to prescribed initial states.

The adequacy of the spin-up was evaluated by comparing modeled end-of-summer snowline elevations with independent field observations and satellite-derived snowline positions. Snowline elevation provides a robust, integrative constraint on late-season snow and firn conditions across the glacier surface. The agreement between modeled and observed snowline elevations, within observational uncertainty, supports the physical plausibility of the initialized snow and firn conditions at the start of the analysis period and their consistency with observed glacier surface states.

Seasonal mass balance components were extracted from the full-year simulations to examine glacier responses to two warm spells and the mid-summer snowfall event (Fig. 8). Model robustness was further assessed by forcing the model with an independent 10-year in-situ temperature and precipitation dataset, calibrated following[50], yielding consistent long-term results and confirming the model's ability to capture interannual glacier–climate variability.

Although SEB models provide a more physically complete description of melt processes, their application requires continuous, on-glacier measurements of radiative and turbulent fluxes, which are unavailable for this site. The AWS-M is located on a lateral moraine and does not fully represent glacier-surface energy conditions, while reanalysis products lack the spatial and temporal resolution required to resolve short-lived extreme events in complex Himalayan terrain. Under these observational constraints, the T-index framework provides a robust and defensible approach for quantifying temperature- and precipitation-driven mass-balance variability during extreme years.

The modeled seasonal mass balance shows pronounced interannual contrasts consistent with in-situ observations (Fig. 8). During spring (1 March–31 May), the modeled mass balance increased from 150 mm w.e. in 2021–22 to 564 mm w.e. in 2022–23 (a 276% increase). Summer (1 June–30 September) mass loss decreased from − 2,311 mm w.e. in 2021–22 to − 1,631 mm w.e. in 2022–23, representing a 28% reduction in ablation.

During the first warm spell (13 March–13 April), the glacier gained only 6.98 mm w.e. in 2021–22, compared with 105 mm w.e. in 2022–23 (≈ 14-fold increase), reflecting stronger spring warming, earlier snowmelt onset, and reduced snow persistence in 2021–22. Consistent with this, cumulative positive degree days during spring 2021–22 were nearly three times higher than in 2023 (Supplementary Figures S4 and S6). During the second warm spell (26 June–13 July), modeled mass loss in 2022–23 (− 281 mm w.e.) was 45% lower than in 2021–22 (− 515 mm w.e.).

A mid-summer snowfall event in July 2022–23 (8–10 July) deposited over 300 mm of snow, sharply increased surface albedo, and resulted in a positive mass balance of approximately 250 mm w.e. between 6 and 24 July. In contrast, the same period in 2021–22 experienced a net mass loss of − 532 mm w.e., corresponding to a ~ 147% turnaround in mass balance.

Overall, these results demonstrate that sub-seasonal extreme events exert a first-order control on annual glacier mass balance. Reduced snowfall in spring and summer accelerates ice exposure, lowers albedo, and intensifies melt, as highlighted in previous studies[16,46,49]. Our findings also reveal that heatwaves and snowfall episodes can strongly influence seasonal mass balance outcomes. Similar patterns have been observed across HMA, where early-season temperature anomalies and shifts in snowfall timing have markedly altered melt dynamics[26,49]. Together, the contrasting responses of 2021–22 and 2022–23 highlight the growing importance of short-lived weather extremes in determining glacier mass balance and underscore the need for high-resolution modeling supported by in-situ observations to improve understanding of glacier–climate interactions in the Himalaya.

Interrelationships between seasonal temperature, precipitation, and mass balance

Correlation analysis over the 2012–2023 period indicates that glacier-wide mass balance at Chhota Shigri Glacier is primarily controlled by summer precipitation and seasonal air temperature, with pronounced inter-seasonal linkages (Fig. 9). Because temperature and precipitation exhibit seasonal covariation, potential multicollinearity

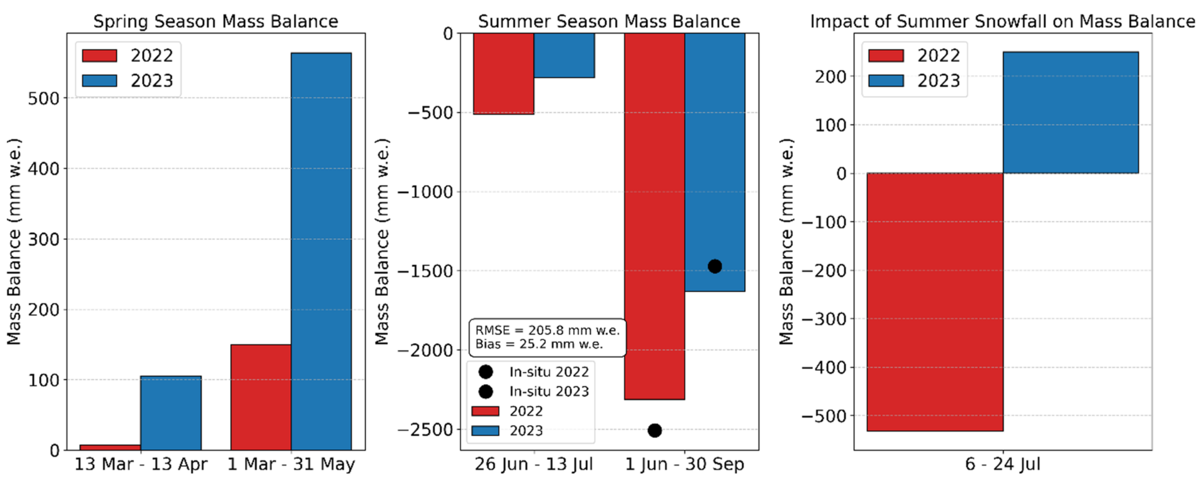

Fig. 8. Modeled mass balance during key seasonal periods for 2022 and 2023. Spring includes two intervals: 13 March to 13 April and the whole spring season (March–May). Summer covers 26 June to 13 July and the full ablation season (June–September). The impact of the 2023 summer snowfall event (6–24 July) is compared with the same period in 2022 to assess seasonal contrasts.

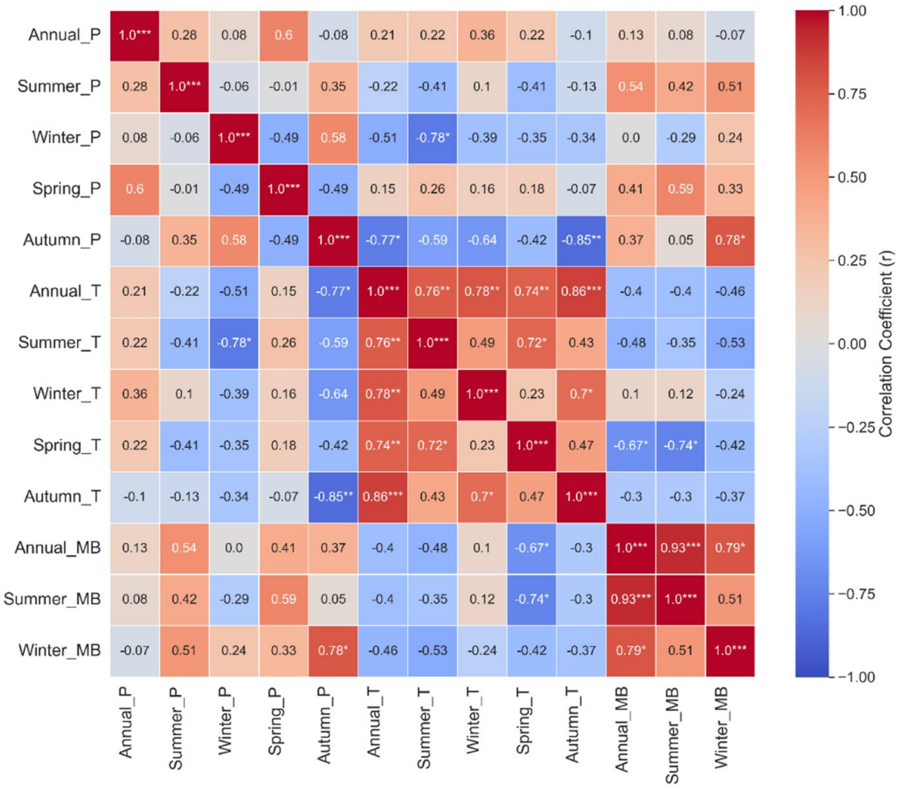

Fig. 9. Correlation matrix of seasonal and annual temperature, precipitation, and glacier mass balance. Colors indicate strength and direction (red: positive, blue: negative) of Pearson correlations. Asterisks denote significance: $p<0.05$ (*), < 0.01 (**), < 0.001 (***).

among predictors was evaluated prior to regression analysis. Variance inflation factors (VIF) computed for seasonal and annual temperature and precipitation variables were moderate (VIF ≈ 4–6), indicating that multicollinearity does not substantially bias the regression coefficients; all predictors were therefore retained. Correlation relationships are interpreted here to identify dominant seasons and underlying physical linkages, rather than to imply the simultaneous use of all variables in a single regression model.

Spring air temperature shows strong negative correlations with both summer mass balance ($r = -0.74$) and annual mass balance ($r = -0.67$), indicating that anomalously warm springs promote early snowmelt, reduce surface albedo, and expose bare ice earlier in the melt season, thereby amplifying summer ablation. Autumn precipitation is strongly correlated with winter mass balance ($r = 0.78$), highlighting the importance of late-autumn snowfall for winter accumulation. Annual mass balance also exhibits positive correlations with both summer ($r = 0.54$) and winter precipitation ($r = 0.51$), reflecting the combined roles of accumulation and precipitation-driven albedo effects.

These patterns are consistent with observations from other Himalayan and Tibetan Plateau glaciers, where enhanced spring warming intensifies summer melt[26], and summer snowfall events suppress ablation by increasing surface reflectivity[16,28,51]. Together, the results extend earlier seasonal assessments[50] by demonstrating that glacier-wide mass balance sensitivity is strongly modulated by inter-seasonal processes. In particular, spring temperature and summer precipitation emerge as critical controls on annual mass-balance variability, underscoring the need for multi-seasonal analyses when assessing glacier responses to extreme weather events.

Quantifying the contribution of summer snowfall to glacier mass balance anomalies

A multiple linear regression analysis between annual glacier-wide mass balance, summer precipitation, and annual temperature (2013–2023) indicates that summer snowfall emerges as the strongest statistical predictor of interannual mass-balance variability ($R^2 = 0.54$, Fig. S7; Supplementary Table S4). The regression model, $MB = -2.30 + 0.0027 \times P_{\text{summer}} - 0.21 \times T_{\text{annual}}$, suggests that each additional 100 mm of summer snowfall is statistically associated with an enhancement of approximately 0.27 m w.e. in annual mass balance, whereas a 1 °C rise in annual temperature is associated with a reduction of about 0.21 m w.e. Given seasonal covariance between temperature and precipitation, these coefficients should be interpreted as statistical sensitivities rather than causal partitioning of mass-balance drivers.

During 2023, the glacier experienced an exceptional July snowfall event, with precipitation approximately 260 mm above the decadal summer mean. Applying the regression-derived sensitivity suggests that this anomaly is statistically consistent with an enhancement of nearly 0.7 m w.e. relative to average summer conditions, representing a substantial fraction of the observed positive annual anomaly in 2022–23. This estimate represents a modeled snowfall-related offset to potential melt rather than a direct physical measurement of glacier gain. Although the observed annual mass balance in 2022–23 was 0.22 m w.e., the statistical relationship indicates that without the anomalous July snowfall, the glacier would likely have experienced a negative annual balance. While statistical significance is limited by the short observational record, the direction and magnitude of the sensitivities are physically consistent with known albedo and precipitation-phase feedbacks. The analysis therefore supports the interpretation that extreme summer snowfall can substantially modulate annual glacier mass balance during warm years, without implying strict causal attribution.

Using the derived sensitivities, each 1 °C increase in annual temperature would statistically require approximately 80 mm of additional summer snowfall to maintain a neutral glacier-wide mass balance. Under projected regional warming of 1.5–2 °C by mid-century[52,53], this scaling implies that summer snowfall would need to increase by ~ 50–160 mm to offset temperature-driven melt enhancement. However, current Himalayan climate projections indicate a shift toward reduced solid precipitation and an increasing proportion of rainfall[54,55]. These results therefore suggest that glaciers such as Chhota Shigri are likely to continue experiencing net mass loss, despite occasional positive-balance years associated with extreme summer snowfall events.

Limitations and broader implications

This study is based on detailed observations from a single, well-instrumented benchmark glacier, and the findings should therefore be interpreted as process-based insights rather than region-wide trends. Two anomalous years do not establish long-term climatic behaviour, and the contrasting mass-balance responses documented here are not intended to represent a persistent regime shift. Instead, they demonstrate how short-duration extreme events can temporarily dominate annual glacier-wide mass balance under favourable local conditions.

While Chhota Shigri Glacier is representative of high-altitude valley glaciers in the western Himalaya in terms of climatic setting and mass-balance regime, extrapolation to other glacier systems requires caution due to climatic heterogeneity, glacier-type variability, and local forcing factors. Future studies integrating high-frequency in-situ observations with geodetic mass-balance estimates and regional remote-sensing analyses across multiple glaciers are required to assess the spatial prevalence, recurrence, and longer-term significance of event-driven mass-balance anomalies.

A limitation of the percentile-based heatwave analysis is the relatively short reference climatology (2010–2021), which coincides with a period of regional warming and may yield slightly elevated percentile thresholds relative to a longer, stationary baseline. Under a warming reference period, percentile thresholds are expected to shift upward $(P_q^{\text{warm}} \geq P_q^{\text{stationary}})$, thereby reducing the probability of exceedance. Consequently, detected heatwave events represent conservative, lower-bound estimates of event frequency and intensity. This limitation primarily affects the absolute magnitude of thresholds rather than the relative identification of extremes, as the same reference period is applied consistently. Consequently, interannual contrasts between 2021 and 22 and 2022–23 remain internally robust.

Summary and conclusion

This study presents the contrasting mass-balance response of Chhota Shigri Glacier, a benchmark valley glacier in the western Himalaya, to two consecutive hydrological years characterised by extreme meteorological conditions. In 2021–22, pronounced spring and summer warming led to a strongly negative annual mass balance (-1.71 ± 0.24 m w.e. a^{-1}), driven by enhanced ablation and reduced snow-cover persistence. In contrast, the 2022–23 hydrological year exhibited a slightly positive mass balance (0.22 ± 0.27 m w.e. a^{-1}), associated with cooler spring conditions and an exceptional mid-summer snowfall event (> 300 mm over three days) that increased surface albedo and substantially reduced melt during the peak ablation period. Although not derived from a full surface energy balance analysis, multiple independent indicators consistently support the interpretation of snowfall-induced melt suppression. This sharp year-to-year contrast underscores the sensitivity of glacier mass balance to short-lived local-scale weather extremes.

Our results demonstrate that seasonal climate variability—particularly spring air temperature and summer precipitation—exerts a dominant control on annual mass balance at Chhota Shigri Glacier, with autumn precipitation also contributing to winter accumulation.

Regression analysis suggests that the July 2023 snowfall anomaly is statistically associated with an enhancement of approximately 0.7 m w.e. in annual mass balance, accounting for nearly 90% of the observed positive anomaly. Given seasonal covariance between temperature and precipitation, this estimate should be interpreted as a statistical sensitivity rather than a strict causal partitioning of mass-balance drivers.

While continued atmospheric warming is expected to drive long-term glacier mass loss, this study demonstrates that short-duration extreme events can temporarily dominate annual mass-balance outcomes at individual glaciers. While magnitudes differ across regions, the mechanisms highlighted here—spring preconditioning through anomalous warming and summer melt suppression through high-altitude snowfall—are relevant to other high-mountain glacier systems where precipitation phase and albedo feedbacks strongly modulate melt. These findings highlight the importance of explicitly accounting for the timing, sequencing, and intensity of extreme temperature and precipitation events in glacier monitoring and modelling frameworks, particularly in data-scarce high-mountain environments where such events can strongly modulate melt processes and associated hydrological impacts.

Methodology

Informed consent was obtained from all identifiable individuals appearing in Fig. 2 for publication of their images in an online open-access journal. All individuals featured have been acknowledged in the manuscript for their field support.

Meteorological data

High-resolution in-situ meteorological observations were used to characterize the atmospheric drivers of glacier mass balance. Air temperature data were obtained from an automatic weather station (AWS-M) installed on a lateral moraine adjacent to Chhota Shigri Glacier at 4,863 m a.s.l. and operating continuously since 2010 (Fig. 1). The AWS-M records air temperature at 30-minute intervals, which were aggregated to hourly and daily values for analysis. Although the station is not located directly on the glacier surface, it provides the longest and most consistent high-elevation temperature record available for the western Himalaya.

Because AWS-M is situated on a lateral moraine, its radiation and albedo measurements do not fully represent glacier-surface energy conditions, particularly during periods of transient snow cover. These variables are therefore interpreted in a relative sense, focusing on temporal changes rather than absolute surface energy fluxes. In particular, short-term increases in albedo following snowfall events are used as a proxy for snow cover persistence and associated changes in the shortwave radiation budget (Supplementary Fig. S1).

Precipitation data were obtained from a single-Alter-shielded Geonor T-200B gauge installed at the base camp (3,844 m a.s.l.) in 2012 (Fig. 1). The gauge records precipitation at 15-minute intervals, which were aggregated to hourly and daily totals for this study.

For long-term climatic context, ERA5-Land reanalysis temperature and precipitation data spanning 1950–2023 were used. Reanalysis data were bias-corrected using linear regression relationships derived from overlapping in-situ AWS-M temperature observations (2010–2023) and Geonor precipitation measurements (2012–2023), following established methods (Supplementary Fig. S8[56,57];. These corrected datasets were used to assess long-term temperature and precipitation anomalies. While ERA5-Land provides valuable large-scale climatic context, it lacks the spatial and temporal resolution required to resolve localized, short-lived extreme events in complex Himalayan terrain. Consequently, interpretation of heatwaves and intense summer snowfall events is primarily based on local in-situ observations.

Near-surface air temperature data from AWS-M were also used to determine precipitation phase, with snowfall identified when temperatures remained below 1.1 °C during precipitation events.

Mass balance measurements

We used in-situ annual and seasonal mass balance data for the two consecutive extreme hydrological years, 2021–22 and 2022–23. The annual glacier–wide mass balance measurements on the Chhota Shigri Glacier have been conducted at the end of September or the beginning of October, using the direct glaciological method since 2002[29,58]. Seasonal mass balance measurements were conducted for the summer (June–September) and winter (October–May) periods. For measuring mass balance, we utilize 2-meter bamboo stakes inserted into the ablation area using a steam drill to depths of 8 to 10 m at the end of each summer. A well-distributed network of approximately 23 bamboo stakes is between 4300 and 4900 m above sea level (m a.s.l.). While the net annual accumulation is assessed in the accumulation area, located between 5150 and 5550 m a.s.l., using six 5–6 snow/firn cores, depending on accessibility.

Observational uncertainty is derived from the in-situ glaciological mass-balance measurement framework described by[29] and includes uncertainties associated with stake readings, snow-density estimation, and spatial extrapolation across elevation bands. Following standard error propagation approaches, model-related and observational uncertainties are combined to obtain the total uncertainty in annual glacier-wide mass balance.

Heatwave and precipitation extremes

The Indian Meteorological Department (IMD) defines a heatwave for hilly regions as a period during which maximum air temperature exceeds the seasonal normal by 4.5–6.4 °C, with severe heatwaves exceeding 6.4 °C. However, no specific definition of a heatwave exists for Himalayan glacierized environments, where local climatic conditions and surface–atmosphere interactions differ markedly from those in lowland regions. Similarly, the World Meteorological Organization (WMO) does not prescribe fixed heatwave thresholds for glaciers, but emphasizes the use of long-term local climatology to identify extreme temperature anomalies. Consequently, percentile-based approaches are commonly adopted to characterize heatwaves in mountainous and glacierized regions[9,59].

To investigate the climatic drivers underlying the contrasting glacier mass-balance responses during the hydrological years 2021–22 and 2022–23, we analysed in-situ meteorological observations from the AWS-M station and precipitation data from the Geonor gauge. Heatwave detection was performed using both daily and hourly percentile-based threshold methods, enabling identification of prolonged warm periods and short-lived extreme temperature events relevant to glacier melt processes.

Let $T_{\max}(d,y)$denote the daily maximum air temperature on calendar day d(month–day) in year y. For each calendar day d, percentile thresholds $P_q\left(d\right)$were computed as:

$$P_q\left(d\right)=\text{quantile}_q\left(\left\{T_{\max}(\,d,y)\mid y\in Y_{\text{ref}}\right\}\right), \quad (1)$$

where $q\in\{90{,}95{,}97.5{,}99\}$ and $Y_{\text{ref}}=$ 2010-2021denotes the reference period. Percentiles were calculated independently for each calendar day using all available observations from the reference years. No temporal smoothing (e.g., ± 7-day moving windows) was applied to the percentile thresholds.

A heatwave day was defined when:

$$T_{\max}(d,y)>P_q\left(d\right). \quad (2)$$

A heatwave event was identified when this condition persisted for at least three consecutive days, with no gaps permitted. Events terminated when the daily maximum temperature fell below the percentile threshold.

Heatwave intensity was quantified as the cumulative positive anomaly above the threshold during the event. The daily temperature record used in this analysis is continuous; therefore, no interpolation or gap-filling was required.

An analogous percentile-based analysis was conducted at the hourly scale to capture short-lived extreme temperature events (Fig. 5). Hourly percentile thresholds were computed using the same reference period, and hourly heatwaves were defined as periods of at least three consecutive hours exceeding the relevant threshold[59].

Precipitation extremes

Daily precipitation records from 2012 to 2023 were analysed to identify extreme precipitation events, with particular emphasis on the July 2023 snowfall event. While the IMD defines heavy rainfall using fixed intensity thresholds, such criteria are less suitable for high-mountain glacierized environments characterized by highly intermittent precipitation and distinct local climatology. Accordingly, and following WMO recommendations, extreme precipitation events were identified using a percentile-based approach.

Let $P(d)$denote daily precipitation totals. Percentile thresholds were computed as:

$$P_q = \text{quantile}_q\left(\{P(d) \mid d \in 2012\text{-}2023\}\right), \tag{3}$$

where $q = 95$and 99. A precipitation day was classified as extreme when $P(d) > P_q$. Extreme precipitation events were defined as one or more consecutive extreme days, with no minimum duration requirement imposed. No temporal smoothing, interpolation, or extrapolation was applied.

Precipitation phase (snow versus rain) was determined using near-surface air temperature, with snowfall identified when air temperature remained below 1.1 °C. The July 2023 event exceeded the 99th percentile and occurred entirely under near-freezing to sub-zero conditions, confirming its classification as an extreme summer snowfall event. The precipitation record used in this analysis is continuous; therefore, no missing-data treatment was required.

Temperature-index modeling

In previous studies, a simplified temperature-index (T-index) model has been successfully applied to Chhota Shigri Glacier to reconstruct long-term mass balance since 1950 using ERA5-Land reanalysis data[31,60]. In this study, we apply the same modelling framework but force it with local in-situ meteorological observations (air temperature and precipitation) to estimate glacier mass balance during the hydrological years 2021–22 and 2022–23, which were characterised by extreme climatic conditions. Modelled mass balance was validated against observed seasonal (summer) mass-balance measurements for the corresponding years, allowing improved representation of seasonal and interannual variability, particularly the impact of heatwave and extreme snowfall events.

The T-index model simulates glacier melt using daily mean air temperature and precipitation as inputs. Melt is calculated as a linear function of positive air temperatures exceeding a threshold and is modulated by degree-day factors (DDFs). Precipitation is partitioned into snowfall and rainfall using a temperature threshold of 1.1 °C, with precipitation falling as snow when $T \leq 1.1\ °C$ and as rain otherwise, following[31,60]. Melt initiation is assumed to occur when air temperature exceeds a threshold of – 0.7 °C, consistent with earlier studies at the site.

Daily air temperature input is derived from AWS-M observations and extrapolated to the glacier hypsometry using observed lapse rates at 50 m elevation intervals. Precipitation input is taken from the Geonor gauge located near the glacier. No additional precipitation correction factor is applied, consistent with previous modelling studies at Chhota Shigri Glacier. Melt at each elevation band is calculated using the positive degree-day (PDD) approach. Daily ablation *a* (mm w.e. d^{-1}) is computed as:

$$a = \{DDF_{S,I,D}.\,(T - T_M) : when T > T_M \\ 0 : when \leq T_M \tag{4}$$

where T is the extrapolated daily mean air temperature (°C) at a given elevation,T_M is the melt threshold temperature (–0.7 °C), and DDF represents the degree-day factor corresponding to the surface type: snow (S), clean ice (I), or debris-covered ice (D). Locally calibrated DDF values of 4.1 mm w.e. °C^{-1} d^{-1} for snow, 8.1 mm w.e. °C^{-1} d^{-1} for clean ice, and 3.6 mm w.e. °C^{-1} d^{-1} for debris-covered ice are adopted, following the calibration presented in[31,50], based on extensive in-situ measurements.

Model calibration

The temperature-index model was calibrated using a 10-year in-situ dataset comprising AWS-derived air temperature and precipitation records together with stake-based seasonal and annual mass-balance observations from Chhota Shigri Glacier. Degree-day factors for snow and ice were adjusted to minimize the difference between modeled and observed seasonal and annual glacier-wide mass balance over the calibration period. Model performance was evaluated against independent stake measurements not used during calibration. All calibrated parameters were subsequently held constant for the simulation of the extreme hydrological years 2021–22 and 2022–23 to ensure internal consistency. The calibration procedure follows the methodology described in[60].

Model uncertainty

Uncertainty in modeled glacier mass balance arises from both parameter uncertainty within the temperature-index model and uncertainty associated with in-situ mass-balance observations. Model uncertainty was quantified following the parametric sensitivity framework of[60], which evaluates the response of simulated mass balance to systematic perturbations in key parameters, including degree-day factors, temperature lapse rates, precipitation gradients, and threshold temperatures, with uncertainty propagated through the model. Based on this framework, the resulting uncertainty in annual glacier-wide mass balance is estimated as ± 0.26 m w.e. for 2021–22 and ± 0.31 m w.e. for 2022–23. Seasonal mass-balance uncertainties are derived consistently from the annual simulations and therefore inherit the same uncertainty structure.

Data availability

Glacier mass balance data are available from the World Glacier Monitoring Service (WGMS): ([https://wgms.ch/](https:/wgms.ch)). ERA5-Land data are available from the Copernicus Climate Data Store: ([https://cds.climate.copernicus.eu/](https:/cds.climate.copernicus.eu)). Other meteorological datasets used in this study will be made available upon reasonable request.

Received: 13 November 2025; Accepted: 4 March 2026
Published online: 29 April 2026

References

1. Hock, R. et al. GlacierMIP – A model intercomparison of global-scale glacier mass-balance models and projections. *J. Glaciol.* **65**, 453–467 (2019).
2. Trewin, B. et al. Headline Indicators for Global Climate Monitoring. *Bull. Am. Meteorol. Soc.* **102**, E20–E37 (2021).
3. Zemp, M. et al. Historically unprecedented global glacier decline in the early 21st century. *J. Glaciol.* **61**, 745–762 (2015).
4. Dussaillant, I. et al. Annual mass changes for each glacier in the world from 1976 to 2023. Preprint at (2024). https://doi.org/10.5194/essd-2024-323
5. Hugonnet, R. et al. Accelerated global glacier mass loss in the early twenty-first century. *Nature* **592**, 726–731 (2021).
6. Tielidze, L. G., Mackintosh, A. N. & Yang, W. Glacier inventories reveal an acceleration of Heard Island glacier loss over recent decades. *Cryosphere* **19**, 2677–2694 (2025).
7. Minobe, S. et al. Global and regional drivers for exceptional climate extremes in 2023–2024: beyond the new normal. *Npj Clim. Atmospheric Sci.* **8**(1), 138 (2025).
8. World Meteorological Organization (WMO). *State of the Global Climate 2024* (World Meteorological Organization, 2025).
9. Cremona, A., Huss, M., Landmann, J. M., Borner, J. & Farinotti, D. European heat waves 2022: contribution to extreme glacier melt in Switzerland inferred from automated ablation readings. *Cryosphere* **17**, 1895–1912 (2023).
10. Voordendag, A., Prinz, R., Schuster, L. & Kaser, G. Brief communication: The Glacier Loss Day as an indicator of a record-breaking negative glacier mass balance in 2022. *Cryosphere* **17**, 3661–3665 (2023).
11. Xu, C. et al. Heatwaves in summer 2022 forces substantial mass loss for Urumqi Glacier 1, China. *J. Glaciol.* **70**, e77 (2024).
12. Alexander, L. V. et al. Global observed changes in daily climate extremes of temperature and precipitation. *J. Geophys. Res. Atmos.* **111**, 2005JD006290 (2006).
13. Frich, P. et al. Observed coherent changes in climatic extremes during the second half of the twentieth century. *Clim. Res.* **19**, 193–212 (2002).
14. Ghanghas, A., Sharma, A., Dey, S. & Merwade, V. How Is Spatial Homogeneity in Precipitation Extremes Changing Globally? *Geophys. Res. Lett.* **50**, e2023GL103233 (2023).
15. Poudel, A., Cuo, L., Gyawali, A. R. & Li, N. Spatiotemporal Patterns of Hydrometeorological Extremes over 1986–2015 in Nepal. *J. Hydrometeorol.* **23**, 573–596 (2022).
16. Azam, M. F. et al. Processes governing the mass balance of Chhota Shigri Glacier (western Himalaya, India) assessed by point-scale surface energy balance measurements. *Cryosphere* **8**, 2195–2217 (2014).
17. Ding, Z., Ha, Y., Huangfu, J. & Zhong, Z. What Distinguishes Summer Extreme Precipitation From Non-Extreme Precipitation Over the Tibetan Plateau? *Geophys Res. Lett* **51**(20), e2024GL111192 (2024).
18. Gupta, V. et al. Hydrometeorological analysis of July-2023 floods in Himachal Pradesh, India. *Nat. Hazards.* **120**, 7549–7574 (2024).
19. Raghuvanshi, A. S. & Agarwal, A. Multiscale dynamics of transient merging between western disturbances and monsoonal lows: Connections to the July 2023 flood in Himachal Pradesh. *Atmospheric Res.* **304**, 107401 (2024).
20. Maussion, F. et al. Precipitation Seasonality and Variability over the Tibetan Plateau as Resolved by the High Asia Reanalysis*. *J. Clim.* **27**, 1910–1927 (2014).
21. Kumar, K. N. et al. Influence of tropical-extratropical interactions on the dynamics of extreme rainfall event: A case study from Indian region. *Dyn. Atmos. Oceans.* **85**, 28–40 (2019).
22. Midhuna, T. M., Dimri, A. P., Suneeth, K. V. & Pattanaik, D. R. Future frequency and intensity of Western Disturbance(s). *Int. J. Climatol.* **43**, 1756–1772 (2023).
23. Hunt, K. M. R. et al. Western disturbances and climate variability: a review of recent developments. *Preprint at.* https://doi.org/10.5194/egusphere-2024-820 (2024).
24. Priya, P., Krishnan, R., Mujumdar, M. & Houze, R. A. Changing monsoon and midlatitude circulation interactions over the Western Himalayas and possible links to occurrences of extreme precipitation. *Clim. Dyn.* **49**, 2351–2364 (2017).
25. Das, S., Kar, N. S. & Bandyopadhyay, S. Glacial lake outburst flood at Kedarnath, Indian Himalaya: a study using digital elevation models and satellite images. *Nat. Hazards.* **77**, 769–786 (2015).
26. Zhu, F. et al. Drivers of the Extreme Early Spring Glacier Melt of 2022 on the Central Tibetan Plateau. *Earth Space Sci.* **11**, e2023EA003297 (2024).
27. Fujita, K. Influence of precipitation seasonality on glacier mass balance and its sensitivity to climate change. *Ann. Glaciol.* **48**, 88–92 (2008).
28. Lin, Q., Chen, J. & Chen, D. Sensitivity of precipitation to glacier changes in the Tibetan Plateau. *J. Hydrol.* **666**, 134862 (2026).
29. Azam, M. F. et al. Reanalysis of the longest mass balance series in Himalaya using a nonlinear model: Chhota Shigri Glacier (India). *Cryosphere* **18**, 5653–5672 (2024).
30. Mandal, A. et al. Understanding the interrelationships among mass balance, meteorology, discharge and surface velocity on Chhota Shigri Glacier over 2002–2019 using in situ measurements. *J. Glaciol.* **66**, 727–741 (2020).
31. Azam, M. F. et al. Reconstruction of the annual mass balance of Chhota Shigri glacier, Western Himalaya, India, since 1969. *Ann. Glaciol.* **55**, 69–80 (2014).
32. Mandal, A. et al. An 11-year record of wintertime snow-surface energy balance and sublimation at 4863 m a.s.l. on the Chhota Shigri Glacier moraine (western Himalaya, India). *Cryosphere* **16**, 3775–3799 (2022).
33. Mohd Farooq Azam. 50 years of Himalayan glacier mass balance monitoring: recommendations in honour of IYGP 2025. Journal of Glaciology, (accepted). (2026).
34. Pratap, B., Oulkar, S. N., Garg, P. K., Sharma, P. & Thamban, M. Mass balance of lake terminating Gepang Gath glacier (western Himalaya, India) and the role of glacier–lake interactions. *J. Glaciol.* **71**, e30 (2025).

35. Azam, M. F. et al. Initial glaciological investigations on a large Himalayan glacier: Drang Drung (Zanskar, Ladakh, India). *J. Glaciol.* **71**, e56 (2025).
36. World Glacier Monitoring Service (WGMS) Fluctuations of Glaciers (FoG) Database. *World Glacier Monit. Service.* **857 MB** https://doi.org/10.5904/WGMS-FOG-2025-02B (2025).
37. Dumont, M. et al. Linking glacier annual mass balance and glacier albedo retrieved from MODIS data. *Cryosphere* **6**, 1527–1539 (2012).
38. Mölg, T., Maussion, F., Yang, W. & Scherer, D. The footprint of Asian monsoon dynamics in the mass and energy balance of a Tibetan glacier. *Cryosphere* **6**, 1445–1461 (2012).
39. Shaw, T. E. et al. Multi-decadal monsoon characteristics and glacier response in High Mountain Asia. *Environ. Res. Lett.* **17**, 104001 (2022).
40. Goodison, B. E., Louie, P. Y. T. & Yang, D. *WMO Solid Precipitation Measurement Intercomparison*. (1998).
41. Kochendorfer, J. et al. The quantification and correction of wind-induced precipitation measurement errors. *Hydrol. Earth Syst. Sci.* **21**, 1973–1989 (2017).
42. Kochendorfer, J. et al. How Well Are We Measuring Snow Post-SPICE? *Bull. Am. Meteorol. Soc.* **103**, E370–E388 (2022).
43. Rasmussen, R. et al. How Well Are We Measuring Snow: The NOAA/FAA/NCAR Winter Precipitation Test Bed. *Bull. Am. Meteorol. Soc.* **93**, 811–829 (2012).
44. Oerlemans, J. & Klok, E. J. (Lisette). Effect of summer snowfall on glacier mass balance. *Ann. Glaciol.* **38**, 97–100 (2004).
45. Bravo, C. et al. An unseasonal atmospheric river drives anomalous summer snow accumulation on glaciers of the subtropical Andes. *Cryosphere* **19**, 1897–1913 (2025).
46. Fujita, K. & Ageta, Y. Effect of summer accumulation on glacier mass balance on the Tibetan Plateau revealed by mass-balance model. *J. Glaciol.* **46**, 244–252 (2000).
47. Che, Y. et al. Energy balance model of mass balance and its sensitivity to meteorological variability on Urumqi River Glacier 1 in the Chinese Tien Shan. *Sci. Rep.* **9**, 13958 (2019).
48. Fugger, S. et al. Understanding monsoon controls on the energy and mass balance of glaciers in the Central and Eastern Himalaya. *Cryosphere* **16**, 1631–1652 (2022).
49. Zhu, Y. et al. High-altitude precipitation controls the mass balance of Pasu Glacier, Karakoram over 2000–2020: A case study based on mass and energy budget. *Adv. Clim. Change Res.* **S167492782500070X** https://doi.org/10.1016/j.accre.2025.03.009 (2025).
50. Srivastava, S., Garg, P. K. & Azam, M. F. Seven Decades of Dimensional and Mass Balance Changes on Dokriani Bamak and Chhota Shigri Glaciers, Indian Himalaya, Using Satellite Data and Modelling. *J. Indian Soc. Remote Sens.* **50**, 37–54 (2022).
51. Immerzeel, W. W., Wanders, N., Lutz, A. F., Shea, J. M. & Bierkens, M. F. P. Reconciling high-altitude precipitation in the upper Indus basin with glacier mass balances and runoff. *Hydrol. Earth Syst. Sci.* **19**, 4673–4687 (2015).
52. Krishnan, R. et al. Unravelling Climate Change in the Hindu Kush Himalaya: Rapid Warming in the Mountains and Increasing Extremes. In *The Hindu Kush Himalaya Assessment* (eds Wester, P., Mishra, A., Mukherji, A., Shrestha, A. B. et al.) 57–97 (Springer International Publishing, 2019). https://doi.org/10.1007/978-3-319-92288-1_3.
53. Calvin, K. *et al. IPCC, 2023: Climate Change 2023: Synthesis Report. Contribution of Working Groups I, II and III to the Sixth Assessment Report of the Intergovernmental Panel on Climate Change [Core Writing Team, H. Lee and J. Romero (Eds.)]. IPCC, Geneva, Switzerland.* https://www.ipcc.ch/report/ar6/syr/ (2023). https://doi.org/10.59327/IPCC/AR6-9789291691647
54. Palazzi, E., Filippi, L. & Von Hardenberg, J. Insights into elevation-dependent warming in the Tibetan Plateau-Himalayas from CMIP5 model simulations. *Clim. Dyn.* **48**, 3991–4008 (2017).
55. Sanjay, J., Krishnan, R., Shrestha, A. B., Rajbhandari, R. & Ren, G. Y. Downscaled climate change projections for the Hindu Kush Himalayan region using CORDEX South Asia regional climate models. *Adv. Clim. Change Res.* **8**, 185–198 (2017).
56. Azam, M. F. & Srivastava, S. Mass balance and runoff modelling of partially debris-covered Dokriani Glacier in monsoon-dominated Himalaya using ERA5 data since 1979. *J. Hydrol.* **590**, 125432 (2020).
57. Zhao, P. & Qian, L. Elevation Correction of ERA5 Reanalysis Temperature over the Qilian Mountains of China. *Atmosphere* **16**, 324 (2025).
58. Wagnon, P. et al. Four years of mass balance on Chhota Shigri Glacier, Himachal Pradesh, India, a new benchmark glacier in the western Himalaya. *J. Glaciol.* **53**, 603–611 (2007).
59. Hutter, H. P., Moshammer, H., Wallner, P., Leitner, B. & Kundi, M. Heatwaves in Vienna: effects on mortality. *Wien Klin. Wochenschr.* **119**, 223–227 (2007).
60. Srivastava, S. & Azam, M. F. Functioning of glacierized catchments in Monsoon and Alpine regimes of Himalaya. *J. Hydrol.* **609**, 127671 (2022).

Acknowledgements
This research was generously supported by the Ministry of Earth Sciences (MOES/PAMC/H&C/131/2019-PC-II) and Space Application Centre (SAC, ISRO). The authors sincerely thank our project assistant, Bhim Bahadur Adhikari, for his invaluable assistance in the field. We would also like to acknowledge and thank Smriti Srivastava and Sachin Kumar Thakur for their dedicated support during the research expedition and throughout the project.

Author contributions
Authors' contributions. HK Investigation, Conceptualization, Formal analysis, Writing – original draft, Visualization - draft. MFA : Funding acquisition, Investigation, Conceptualization, Writing – review & editing. AH: Investigation, Writing – review & editing.

Funding
There was funding available for this work.

Declarations

Competing interests
The authors declare no competing interests.

Consent for publication
Written informed consent was obtained from all individuals whose identifiable images appear in Fig. 2.

Additional information

Supplementary Information The online version contains supplementary material available at https://doi.org/10.1038/s41598-026-43456-1.

Correspondence and requests for materials should be addressed to M.F.A.